Acta Cryst E CRYSTALLOGRAPHIC COMMUNICATIONS

ISSN 2056-9890

Synthesis and crystal structure of the mixed-valent $Te^{IV/VI}$ compound $PbTe_3O_8$

Matthias Weil*

Institute for Chemical Technologies and Analytics, Division of Applied Solid State Chemistry, TU Wien, Getreidemarkt 9/E164-05-1, A-1060, Vienna, Austria. *Correspondence e-mail: matthias.weil@tuwien.ac.at

Received 6 October 2026
Accepted 22 October 2026

Edited by K. V. Domasevitch, National Taras Shevchenko University of Kyiv, Ukraine

Keywords: crystal structure; isotypism; mixed-valent compound; structural comparison.

CCDC reference: 2597291

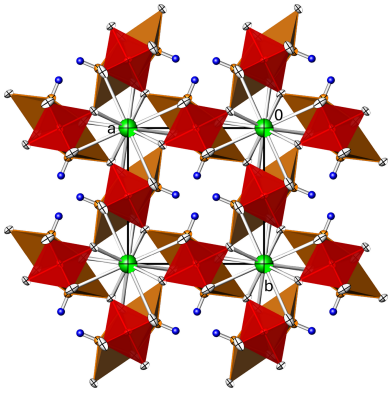
Supporting information: this article has supporting information at journals.iucr.org/e

The crystal structure of the mixed-valent compound $PbTe_3O_8$ (= $Pb^{II}Te^{IV}{}_2Te^{VI}O_8$), lead(II) bis[oxidotellurate(IV)] tellurate(VI), is isotypic with that of $SrTe_3O_8$. It comprises $^1_\infty[Te_3O_8]^{2-}$ chains sharing O atoms to form a framework with two types of square channels extending parallel to [001]. The smaller channels (diameter ~4 Å) are occupied by 12-coordinate Pb^{II} atoms in the centre of the channel, whereas the slightly larger channels (diameter ~4.5 Å) accommodate the stereoactive $5s^2$ electron lone pair of Te^{IV}.

1. Chemical context

In addition to the interest in the crystal-chemical peculiarities of compounds containing Pb^{II} and Te^{IV} atoms that are characterized by their lone pair electrons (Walsh *et al.*, 2011), phases in the Pb/Te/O system are also relevant in terms of application-related problems. This applies, for example, to PbTe-based thermoelectrics (Kanatzidis, 2010) or to Pb/Te/O-based high-refractive index glasses (Alazoumi *et al.*, 2018), where they can occur as unwanted surfacial oxidation products and as (re)crystallized phases, respectively. It is therefore important to have a thorough knowledge of the formation conditions and crystal structures of such phases.

Taking lead(II) oxidotellurate(VI), $PbTeO_4$, as an example, polycrystalline material from it was prepared at a temperature of 973 K and a pressure of 3000 atm (Sleight *et al.*, 1972). In an attempt to grow $PbTeO_4$ crystals under more moderate hydrothermal conditions following a modified procedure reported by Mathers & Graham (1929), crystals of the so far unknown compound $PbTe_3O_8$ were obtained serendipitously, and its crystal structure is reported in the present communication. As it turned out, $PbTeO_4$ can only be prepared at higher pressure and temperature conditions (Hladik *et al.*, 2024).



2. Structural commentary

$PbTe_3O_8$ expands our knowledge of ternary phases in the Pb/Te/O system (all contain lead solely in oxidation state +II), of which the following are currently known. For oxidotellurates(IV): α-$PbTeO_3$ (Mariolacos, 1969; Zavodnik *et al.*, 2008; Missen *et al.*, 2019*b*), β-$PbTeO_3$ (Sciau *et al.*, 1986; Ma *et al.*, 2017; Weil *et al.*, 2018), γ-$PbTeO_3$ (Weil *et al.*, 2018; Kampf *et al.*, 2022), $Pb_2Te_3O_8$ (Dewan *et al.*, 1978; Champarnaud-Mesjard *et al.*, 2001), $PbTe_5O_{11}$ (Oufkir *et al.*, 2001); for oxidotellurates(VI): $PbTeO_4$ (Hladik *et al.*, 2024), Pb_2TeO_5 (Kampf *et al.*, 2010; Artner & Weil, 2013), Pb_5TeO_8 (Artner & Weil, 2013). This makes $PbTe_3O_8$ the first mixed-valent $Te^{IV/VI}$ compound (= $Pb^{II}Te^{IV}{}_2Te^{VI}O_8$) in the ternary Pb/Te/O system.

OPEN ACCESS
Published under a CC BY 4.0 licence

It belongs to class I of the Robin & Day (1967) classification, with the different valence states each clearly located on their own atomic sites.

The crystal structure of $PbTe_3O_8$ is isotypic with that of $SrTe_3O_8$ (Barrier *et al.*, 2006; Weil & Stöger, 2007). It can be considered as being composed of $^1_\infty[Te_2^{IV}Te^{VI}O_8]^{2-}$ chains, with adjacent chains sharing O atoms to form a framework with two types of square channels extending parallel to [001] (Fig. 1).

The $^1_\infty[Te_2^{IV}Te^{VI}O_8]^{2-}$ chains consist of $\{Te1_2O_8\}$ double polyhedra, which are formed by two symmetry-related $\{Te1^{IV}O_5\}$ pyramids (Te1, site symmetry *m*..), and of $\{Te2^{VI}O_6\}$ octahedra (Te2, 2/*m*..) by sharing corners and edges (Fig. 2). In the framework, each $\{Te2O_6\}$ octahedron is connected to four $\{Te1_2O_8\}$ double polyhedra, two *via* shared edges and two *via* shared corners, and each $\{Te1_2O_8\}$ double polyhedron is connected in the same way to four $\{Te2O_6\}$ octahedra. The $\{Te1O_5\}$ pyramid deviates somewhat from an ideal square-pyramidal coordination geometry (the τ_5 index is 0.23, with extreme values of 0 for ideal square-pyramidal and 1 for ideal trigonal-bipyramidal geometry; Addison *et al.*, 1984). The Te—O bond lengths span a range from 1.948 (10) to 2.170 (9) Å (Table 1). The $\{Te2O_6\}$ octahedron shows no variance in bond lengths (Table 1) and only minor angular distortions for the equatorial O atoms [range 85.2 (4)–94.8 (4)°]. All Te—O bond lengths are in characteristic ranges for tetra- and hexavalent tellurium atoms (Christy *et al.*, 2016). The *LPLoc* software (Hamani *et al.*, 2020) revealed the position of the presumed $5s^2$ electron lone pair at the $Te1^{IV}$ site with resulting fractional coordinates of x = 0.49158, y = 0.35089, z = 0. The radius of the electron lone pair was calculated to be 1.03 Å with a distance of 1.027 Å from the Te1 position. The electron lone pair protrudes into the larger of the two channels (diameter ∼4.5 Å), and thus is stereochemically active, as shown in Fig. 1.

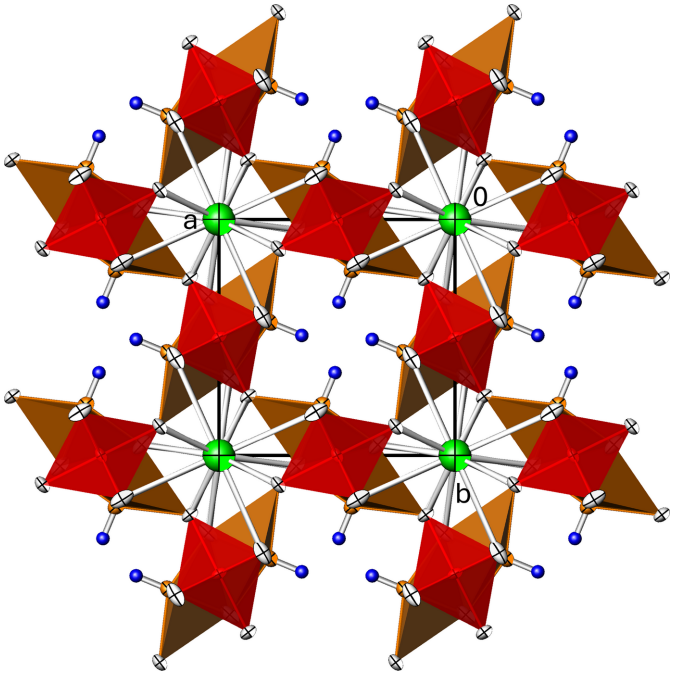


Figure 1
View of the crystal structure of $PbTe_3O_8$ in a projection along [001]. Displacement ellipsoids are drawn at the 90% probability level. Colour code: Pb green, O colourless, $\{Te1O_5\}$ square pyramid orange, $\{Te2O_6\}$ octahedron red; the $5s^2$ lone pair at the Te1 site is indicated as a blue sphere of arbitrary size.

Table 1
Selected bond lengths (Å).

Pb1—O2	2.570 (7)	Te1—O1	2.080 (7)
Pb1—O3^{i}	2.842 (8)	Te1—O1^{iii}	2.080 (7)
Pb1—O1	3.147 (8)	Te1—O2	2.170 (9)
Te1—O3^{ii}	1.948 (10)	Te2—O1^{iv}	1.927 (7)
Te1—O3	2.027 (9)	Te2—O2	1.927 (9)

Symmetry codes: (i) $x-1, y, z$; (ii) $-x+1, -y, -z$; (iii) $x, y, -z$; (iv) $y, -x+1, z-\frac{1}{2}$.

The Pb^{II} cation is located in the smaller channel (diameter ∼4 Å, Fig. 1). It exhibits site symmetry $\overline{4}$.. and has a coordination number of 12, with three groups of short, medium and long Pb—O bond lengths (Table 1). The corresponding $[PbO_{12}]$ coordination polyhedron was analysed using the *Polynator* program (Link & Niewa, 2023). It has a volume of 52.82 $Å^3$ and can be described as a distorted cuboctahedron that differs from the ideal polyhedron (point group $\overline{4}2m$) by a δ value (Link & Niewa, 2023) of 5.736. The average $Pb^{[12]}$—O distance (2.853 Å) is in good agreement with the value of 2.827 (113) Å provided by Gagné & Hawthorne (2018). Localization of the electron lone pair at the Pb^{II} site using *LPLoc* shows that it is situated directly at the metal site (calculated lone pair radius 1.16 Å) and apparently exhibits no stereochemical activity.

A quantitative comparison between the isotypic MTe_3O_8 (M = Pb, Sr) structures was carried out using the *compstru* software (de la Flor *et al.*, 2016), available at the Bilbao Crystallographic Server (Aroyo *et al.*, 2006). The absolute distances between paired atoms are 0 Å for Pb1/Sr1, 0 Å for Te2, 0.0235 Å for Te1, 0.0247 Å for O3, 0.0252 Å for O1, and 0.0600 Å for O2; the arithmetic mean of the distance between paired atoms is 0.0264 Å. The degree of lattice distortion (0.0070), and the low value for the measure of similarity

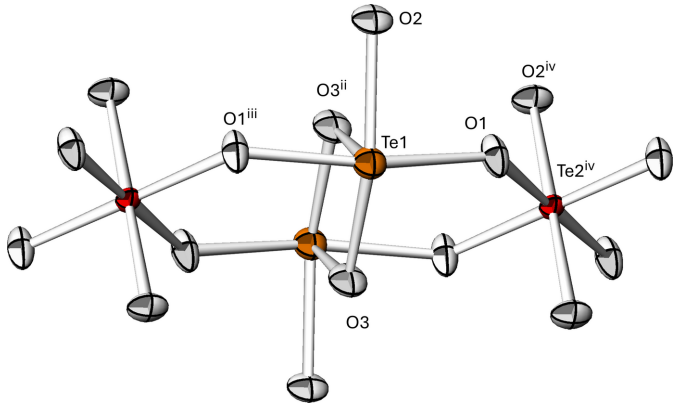


Figure 2
Part of a $^1_\infty[Te_2^{IV}Te^{VI}O_8]^{2-}$ chain. Displacement ellipsoids are drawn at the 90% probability level. Symmetry codes refer to Table 1.

(0.024) indicate a high degree of simiularity for the two crystal structures.

In addition to the two isotypic $M\mathrm{Te_3O_8}$ (M = Pb, Sr) structures, there is another compound with the same formula type (M = Ca) that occurs in nature as the rare mineral carlfriesite. Its monoclinic crystal structure (Effenberger *et al.*, 1978; Missen *et al.*, 2019*a*) can also be described as a nanoporous framework, although it exhibits a different topology for the $[\mathrm{Te_2^{IV}Te^{VI}O_8}]^{2-}$ anion. Here, the metal cation is situated in slightly larger channels with a diameter of approximately 6 Å and exhibits a coordination number of eight with a distorted tetragonal antiprismatic oxygen coordination.

3. Synthesis and crystallization

The chemicals were supplied by Merck and were used without further purification. Equimolar amounts of $\mathrm{PbO_2}$ and $\mathrm{TeO_2}$ (total load 0.3 g) were thoroughly mixed and placed in a Teflon container. The container was filled to about two-thirds of its inner volume (5 ml) with water, closed with a Teflon lid and placed in a steel autoclave, which was heated at 483 K for two days. The greyish solid product was filtered off and washed with water and ethanol. A few colourless crystals with a rod-like form of the title compound were isolated under a polarising microscope. Qualitative phase analysis of the bulk product from laboratory X-ray powder diffraction data revealed the starting materials $\mathrm{TeO_2}$ and $\mathrm{PbO_2}$ as well as $\mathrm{PbTe_3O_8}$ as products, together with unassigned reflections. This shows that, in a redox reaction, parts of $\mathrm{Pb^{IV}}$ and $\mathrm{Te^{IV}}$ have reacted to form $\mathrm{Pb^{II}}$ and $\mathrm{Te^{VI}}$.

4. Refinement

Crystal data, data collection and structure refinement details are summarized in Table 2. For better comparison with isotypic $\mathrm{SrTe_3O_8}$ (Weil & Stöger, 2007), the same atom numbering scheme and starting coordinates for refinement were used. The residual maximum and minimum difference-electron densities are located 0.61 Å from Te2 and 0.49 Å from Pb1, respectively.

Compared with the other atoms, the displacement parameters of the Pb site are large. The same phenomenon is observed in the isotypic Sr structure (Weil & Stöger, 2007). We assume that this property is characteristic of this type of structure and is primarily caused by the position of the metal site within the large pores. It is also possible that the Pb site shows positional order around the $\overline{4}$ axis or is under-occupied with a potential $\mathrm{Pb^{II/IV}}$ co-occupation, but this cannot be conclusively demonstrated by the available X-ray data. To obtain a more detailed picture, supplementary analytical data are required, for example through wet chemical methods or microprobe analysis.

Table 2
Experimental details.

Crystal data	
Chemical formula	$\mathrm{PbTe_3O_8}$
M_r	717.99
Crystal system, space group	Tetragonal, $P4_2/m$
Temperature (K)	296
a, c (Å)	6.9345 (3), 6.7369 (4)
V (Å^3)	323.96 (3)
Z	2
Radiation type	Mo $K\alpha$
μ (mm^{-1})	39.29
Crystal size (mm)	0.10 × 0.02 × 0.01
Data collection	
Diffractometer	Bruker APEXII CCD
Absorption correction	Multi-scan (*SADABS*; Krause *et al.*, 2015)
T_{min}, T_{max}	0.155, 0.349
No. of measured, independent and observed [$I > 2\sigma(I)$] reflections	7237, 514, 499
R_{int}	0.031
$(\sin\theta/\lambda)_{max}$ (Å^{-1})	0.702
Refinement	
$R[F^2 > 2\sigma(F^2)]$, $wR(F^2)$, S	0.037, 0.112, 1.12
No. of reflections	514
No. of parameters	34
$\Delta\rho_{max}$, $\Delta\rho_{min}$ (e Å^{-3})	3.82, −4.85

Computer programs: *APEX3* and *SAINT* (Bruker, 2018), *SHELXL* (Sheldrick, 2015), *ATOMS* (Dowty, 2006) and *publCIF* (Westrip, 2010).

Acknowledgements

The X-ray Centre of TU Wien is acknowledged for providing access to instrumentation and analysis software and TU Wien Bibliothek for financial support through its Open Access Funding Program.

References

Addison, A. W., Rao, T. N., Reedijk, J., van Rijn, J. & Verschoor, G. C. (1984). *J. Chem. Soc. Dalton Trans.* pp. 1349–1356.
Alazoumi, S. H., Sidek, H. A. A., El-Mallawany, R., Kamari, H. M., Zaid, M. H. M. & Ali, E. A. G. E. (2018). *Appl. Phys. A* **124**, 845.
Aroyo, M. I., Perez-Mato, J. M., Capillas, C., Kroumova, E., Ivantchev, S., Madariaga, G., Kirov, A. & Wondratschek, H. (2006). *Z. Kristallogr.* **221**, 15–27.
Artner, C. & Weil, M. (2013). *J. Solid State Chem.* **199**, 240–247.
Barrier, N., Malo, S., Hernandez, O., Hervieu, M. & Raveau, B. (2006). *J. Solid State Chem.* **179**, 3484–3488.
Bruker (2018). *APEX3* and *SAINT*. Bruker AXS Inc., Madison, Wisconsin, USA
Champarnaud-Mesjard, J. C., Thomas, P., Colas-Dutreilh, M. & Oufkir, A. (2001). *Z. Kristallogr. New Cryst. Struct.* **216**, 185–186.
Christy, A. G., Mills, S. J. & Kampf, A. R. (2016). *Mineral. Mag.* **80**, 415–545.
Dewan, J. C., Edwards, A. J., Jones, G. R. & Young, I. M. (1978). *J. Chem. Soc. Dalton Trans.* pp. 1528–1532.
Dowty, E. (2006). *ATOMS for Windows*. Shape Software, Kingsport, Tennessee, USA.
Effenberger, H., Zemann, J. & Mayer, H. (1978). *Am. Mineral.* **63**, 847–852.
Flor, G. de la, Orobengoa, D., Tasci, E., Perez-Mato, J. M. & Aroyo, M. I. (2016). *J. Appl. Cryst.* **49**, 653–664.
Gagné, O. C. & Hawthorne, F. C. (2018). *Acta Cryst.* B**74**, 79–96.
Hamani, D., Masson, O. & Thomas, P. (2020). *J. Appl. Cryst.* **53**, 1243–1251.
Hladik, M., Penz, A., Purtscher, F. R. S., Hofer, T. S., Heymann, G. & Weil, M. (2024). *Dalton Trans.* **53**, 19214–19225.
Kampf, A. R., Housley, R. M., Mills, S. J., Marty, J. & Thorne, B. (2010). *Am. Mineral.* **95**, 1329–1336.

Kampf, A. R., Missen, O. P., Mills, S. J., Ma, C., Housley, R. M., Chorazewicz, M., Marty, J., Coolbaugh, M. & Momma, K. (2022). *Can. Mineral.* **60**, 805–814.
Kanatzidis, M. G. (2010). *Chem. Mater.* **22**, 648–659.
Krause, L., Herbst-Irmer, R., Sheldrick, G. M. & Stalke, D. (2015). *J. Appl. Cryst.* **48**, 3–10.
Link, L. & Niewa, R. (2023). *J. Appl. Cryst.* **56**, 1855–1864.
Ma, Y., Wang, W., Liu, Q., Zhang, L., Lei, L., Zhang, L. & Liu, Z. (2017). *Solid State Commun.* **260**, 1–5.
Mariolacos, K. (1969). *Anz. Oesterr. Akad. Wiss. Math. Naturwiss. Kl.* **106**, 129–131.
Mathers, F. C. & Graham, F. V. (1929). *J. Am. Chem. Soc.* **51**, 3225–3228.
Missen, O. P., Kampf, A. R., Mills, S. J., Housley, R. M., Spratt, J., Welch, M. D., Coolbaugh, M. F., Marty, J., Chorazewicz, M. & Ferraris, F. (2019*a*). *Mineral. Mag.* **83**, 539–549.
Missen, O. P., Rumsey, M. S., Kampf, A. R., Mills, S. J., Back, M. E. & Spratt, J. (2019*b*). *Mineral. Mag.* **83**, 791–797.
Oufkir, A., Dutreilh, M., Thomas, P., Champarnaud-Mesjard, J. C., Marchet, P. & Frit, B. (2001). *Mater. Res. Bull.* **36**, 693–703.
Robin, M. B. & Day, P. (1967). *Adv. Inorg. Chem. Radiochem.* **10**, 247–422.
Sciau, P., Lapasset, J. & Moret, J. (1986). *Acta Cryst.* C**42**, 1688–1690.
Sheldrick, G. M. (2015). *Acta Cryst.* C**71**, 3–8.
Sleight, A. W., Foris, C. M. & Licis, M. S. (1972). *Inorg. Chem.* **11**, 1157–1158.
Walsh, A., Payne, D. J., Egdell, R. G. & Watson, G. W. (2011). *Chem. Soc. Rev.* **40**, 4455–4463.
Weil, M., Shirkhanlou, M., Füglein, E. & Libowitzky, E. (2018). *Crystals* **8**, 51.
Weil, M. & Stöger, B. (2007). *Acta Cryst.* E**63**, i116–i118.
Westrip, S. P. (2010). *J. Appl. Cryst.* **43**, 920–925.
Zavodnik, V. E., Ivanov, S. A. & Stash, A. I. (2008). *Acta Cryst.* E**64**, i16.

supporting information

Acta Cryst. (2026). E**82**, 1342-1345 [https://doi.org/10.1107/S2056989026010996]

Synthesis and crystal structure of the mixed-valent $Te^{IV/VI}$ compound $PbTe_3O_8$

Matthias Weil

Computing details

Lead(II) bis[oxidotellurate(IV)] tellurate(VI)

Crystal data

$PbTe_3O_8$
M_r = 717.99
Tetragonal, $P4_2/m$
a = 6.9345 (3) Å
c = 6.7369 (4) Å
V = 323.96 (3) Å^3
Z = 2
$F(000)$ = 604
D_x = 7.360 Mg m^{-3}
Mo $K\alpha$ radiation, λ = 0.71073 Å
Cell parameters from 4370 reflections
θ = 3.0–29.4°
μ = 39.29 mm^{-1}
T = 296 K
Fragment, colourless
0.10 × 0.02 × 0.01 mm

Data collection

Bruker APEXII CCD diffractometer
ω– and φ–scans
Absorption correction: multi-scan (*SADABS*; Krause *et al.*, 2015)
T_{min} = 0.155, T_{max} = 0.349
7237 measured reflections
514 independent reflections
499 reflections with $I > 2\sigma(I)$
R_{int} = 0.031
θ_{max} = 29.9°, θ_{min} = 2.9°
h = −9→9
k = −9→9
l = −9→9

Refinement

Refinement on F^2
Least-squares matrix: full
$R[F^2 > 2\sigma(F^2)]$ = 0.037
$wR(F^2)$ = 0.112
S = 1.12
514 reflections
34 parameters
0 restraints
Primary atom site location: isomorphous structure methods
$w = 1/[\sigma^2(F_o^2) + (0.0619P)^2 + 13.4507P]$ where $P = (F_o^2 + 2F_c^2)/3$
$(\Delta/\sigma)_{max} < 0.001$
$\Delta\rho_{max}$ = 3.82 e Å^{-3}
$\Delta\rho_{min}$ = −4.85 e Å^{-3}

Special details

Geometry. All esds (except the esd in the dihedral angle between two l.s. planes) are estimated using the full covariance matrix. The cell esds are taken into account individually in the estimation of esds in distances, angles and torsion angles; correlations between esds in cell parameters are only used when they are defined by crystal symmetry. An approximate (isotropic) treatment of cell esds is used for estimating esds involving l.s. planes.

Fractional atomic coordinates and isotropic or equivalent isotropic displacement parameters (Å²)

	x	*y*	*z*	U_{iso}*/U_{eq}
Pb1	0.000000	0.000000	0.250000	0.0409 (4)
Te1	0.43446 (12)	0.21418 (12)	0.000000	0.0105 (3)
Te2	0.000000	0.500000	0.000000	0.0066 (3)
O1	0.4112 (10)	0.1842 (10)	0.3063 (10)	0.0125 (12)
O2	0.1237 (14)	0.2511 (13)	0.000000	0.0111 (17)
O3	0.6731 (15)	0.0454 (14)	0.000000	0.0129 (18)

Atomic displacement parameters (Å²)

	U^{11}	U^{22}	U^{33}	U^{12}	U^{13}	U^{23}
Pb1	0.0373 (4)	0.0373 (4)	0.0480 (7)	0.000	0.000	0.000
Te1	0.0105 (4)	0.0101 (4)	0.0109 (4)	0.0020 (3)	0.000	0.000
Te2	0.0086 (5)	0.0052 (5)	0.0061 (5)	0.0025 (3)	0.000	0.000
O1	0.019 (3)	0.012 (3)	0.007 (3)	0.007 (2)	0.001 (2)	0.001 (2)
O2	0.009 (4)	0.007 (4)	0.017 (4)	0.003 (3)	0.000	0.000
O3	0.012 (4)	0.013 (4)	0.014 (4)	0.007 (3)	0.000	0.000

Geometric parameters (Å, º)

Pb1—O2^{i}	2.570 (7)	Te1—O3^{vii}	1.948 (10)
Pb1—O2^{ii}	2.570 (7)	Te1—O3	2.027 (9)
Pb1—O2^{iii}	2.570 (7)	Te1—O1	2.080 (7)
Pb1—O2	2.570 (7)	Te1—O1^{x}	2.080 (7)
Pb1—O3^{iv}	2.842 (8)	Te1—O2	2.170 (9)
Pb1—O3^{v}	2.842 (8)	Te2—O1^{iv}	1.927 (7)
Pb1—O3^{vi}	2.842 (8)	Te2—O1^{xi}	1.927 (7)
Pb1—O3^{vii}	2.842 (8)	Te2—O1^{ix}	1.927 (7)
Pb1—O1	3.147 (8)	Te2—O1^{xii}	1.927 (7)
Pb1—O1^{viii}	3.147 (8)	Te2—O2	1.927 (9)
Pb1—O1^{ii}	3.147 (7)	Te2—O2^{xiii}	1.927 (9)
Pb1—O1^{ix}	3.147 (7)		
O2^{i}—Pb1—O2^{ii}	115.43 (15)	O1—Pb1—O1^{ii}	90.83 (3)
O2^{i}—Pb1—O2^{iii}	115.43 (15)	O1^{viii}—Pb1—O1^{ii}	90.83 (3)
O2^{ii}—Pb1—O2^{iii}	98.1 (3)	O2^{i}—Pb1—O1^{ix}	113.5 (2)
O2^{i}—Pb1—O2	98.1 (3)	O2^{ii}—Pb1—O1^{ix}	131.0 (2)
O2^{ii}—Pb1—O2	115.43 (15)	O2^{iii}—Pb1—O1^{ix}	60.1 (2)
O2^{iii}—Pb1—O2	115.43 (15)	O2—Pb1—O1^{ix}	56.1 (2)
O2^{i}—Pb1—O3^{iv}	165.0 (3)	O3^{iv}—Pb1—O1^{ix}	52.7 (2)
O2^{ii}—Pb1—O3^{iv}	78.6 (3)	O3^{v}—Pb1—O1^{ix}	60.3 (2)
O2^{iii}—Pb1—O3^{iv}	54.6 (3)	O3^{vi}—Pb1—O1^{ix}	138.5 (2)
O2—Pb1—O3^{iv}	79.10 (19)	O3^{vii}—Pb1—O1^{ix}	110.6 (2)
O2^{i}—Pb1—O3^{v}	54.6 (3)	O1—Pb1—O1^{ix}	90.83 (3)
O2^{ii}—Pb1—O3^{v}	165.0 (3)	O1^{viii}—Pb1—O1^{ix}	90.83 (3)
O2^{iii}—Pb1—O3^{v}	79.10 (19)	O1^{ii}—Pb1—O1^{ix}	166.2 (3)

O2—Pb1—O3^{v}	78.6 (3)	O3^{vii}—Te1—O3	77.2 (5)
O3^{iv}—Pb1—O3^{v}	110.57 (12)	O3^{vii}—Te1—O1	83.0 (2)
O2^{i}—Pb1—O3^{vi}	79.10 (19)	O3—Te1—O1	90.32 (18)
O2^{ii}—Pb1—O3^{vi}	54.6 (3)	O3^{vii}—Te1—O1^{x}	83.0 (2)
O2^{iii}—Pb1—O3^{vi}	78.6 (3)	O3—Te1—O1^{x}	90.32 (18)
O2—Pb1—O3^{vi}	165.0 (3)	O1—Te1—O1^{x}	165.5 (4)
O3^{iv}—Pb1—O3^{vi}	107.3 (2)	O3^{vii}—Te1—O2	74.3 (4)
O3^{v}—Pb1—O3^{vi}	110.57 (12)	O3—Te1—O2	151.5 (4)
O2^{i}—Pb1—O3^{vii}	78.6 (3)	O1—Te1—O2	86.3 (2)
O2^{ii}—Pb1—O3^{vii}	79.10 (19)	O1^{x}—Te1—O2	86.3 (2)
O2^{iii}—Pb1—O3^{vii}	165.0 (3)	O1^{iv}—Te2—O1^{xi}	180.0
O2—Pb1—O3^{vii}	54.6 (3)	O1^{iv}—Te2—O1^{ix}	94.8 (4)
O3^{iv}—Pb1—O3^{vii}	110.57 (12)	O1^{xi}—Te2—O1^{ix}	85.2 (4)
O3^{v}—Pb1—O3^{vii}	107.3 (2)	O1^{iv}—Te2—O1^{xii}	85.2 (4)
O3^{vi}—Pb1—O3^{vii}	110.57 (12)	O1^{xi}—Te2—O1^{xii}	94.8 (4)
O2^{i}—Pb1—O1	131.0 (2)	O1^{ix}—Te2—O1^{xii}	180.0 (4)
O2^{ii}—Pb1—O1	56.1 (2)	O1^{iv}—Te2—O2	89.5 (3)
O2^{iii}—Pb1—O1	113.5 (2)	O1^{xi}—Te2—O2	90.5 (3)
O2—Pb1—O1	60.1 (2)	O1^{ix}—Te2—O2	90.5 (3)
O3^{iv}—Pb1—O1	60.3 (2)	O1^{xii}—Te2—O2	89.5 (3)
O3^{v}—Pb1—O1	138.5 (2)	O1^{iv}—Te2—O2^{xiii}	90.5 (3)
O3^{vi}—Pb1—O1	110.6 (2)	O1^{xi}—Te2—O2^{xiii}	89.5 (3)
O3^{vii}—Pb1—O1	52.7 (2)	O1^{ix}—Te2—O2^{xiii}	89.5 (3)
O2^{i}—Pb1—O1^{viii}	60.1 (2)	O1^{xii}—Te2—O2^{xiii}	90.5 (3)
O2^{ii}—Pb1—O1^{viii}	113.5 (2)	O2—Te2—O2^{xiii}	180.0
O2^{iii}—Pb1—O1^{viii}	56.1 (2)	Te2^{xiv}—O1—Te1	135.5 (3)
O2—Pb1—O1^{viii}	131.0 (2)	Te2^{xiv}—O1—Pb1	95.9 (3)
O3^{iv}—Pb1—O1^{viii}	110.6 (2)	Te1—O1—Pb1	89.5 (2)
O3^{v}—Pb1—O1^{viii}	52.7 (2)	Te2—O2—Te1	123.2 (5)
O3^{vi}—Pb1—O1^{viii}	60.3 (2)	Te2—O2—Pb1^{i}	117.3 (3)
O3^{vii}—Pb1—O1^{viii}	138.5 (2)	Te1—O2—Pb1^{i}	104.6 (3)
O1—Pb1—O1^{viii}	166.2 (3)	Te2—O2—Pb1	117.3 (3)
O2^{i}—Pb1—O1^{ii}	56.1 (2)	Te1—O2—Pb1	104.6 (3)
O2^{ii}—Pb1—O1^{ii}	60.1 (2)	Pb1^{i}—O2—Pb1	81.9 (3)
O2^{iii}—Pb1—O1^{ii}	131.0 (2)	Te1^{vii}—O3—Te1	102.8 (5)
O2—Pb1—O1^{ii}	113.5 (2)	Te1^{vii}—O3—Pb1^{xv}	101.7 (3)
O3^{iv}—Pb1—O1^{ii}	138.5 (2)	Te1—O3—Pb1^{xv}	135.7 (3)
O3^{v}—Pb1—O1^{ii}	110.6 (2)	Te1^{vii}—O3—Pb1^{vii}	101.7 (3)
O3^{vi}—Pb1—O1^{ii}	52.7 (2)	Te1—O3—Pb1^{vii}	135.7 (3)
O3^{vii}—Pb1—O1^{ii}	60.3 (2)	Pb1^{xv}—O3—Pb1^{vii}	72.7 (2)

Symmetry codes: (i) −*x*, −*y*, −*z*; (ii) *y*, −*x*, −*z*+1/2; (iii) −*y*, *x*, *z*+1/2; (iv) *y*, −*x*+1, −*z*+1/2; (v) *x*−1, *y*, *z*; (vi) −*y*, *x*−1, *z*+1/2; (vii) −*x*+1, −*y*, −*z*; (viii) −*x*, −*y*, *z*; (ix) −*y*, *x*, −*z*+1/2; (x) *x*, *y*, −*z*; (xi) −*y*, *x*, *z*−1/2; (xii) *y*, −*x*+1, *z*−1/2; (xiii) −*x*, −*y*+1, −*z*; (xiv) −*y*+1, *x*, *z*+1/2; (xv) *x*+1, *y*, *z*.